Int. J. Electrochem. Sci., 14 **(2019)** 10153 – 10161, doi: 10.20964/2019.11.24

International Journal of
ELECTROCHEMICAL
SCIENCE
www.electrochemsci.org

Short Communication

Study on the Properties of $LiMn_2O_4$/ $Li_{1.5}Al_{0.5}Ge_{1.5}(PO_4)_3$ Composite Cathode Materials

Xinghua Liang[1,2], *Qiuman Wu*[1,*], *Lingxiao Lan* [1,*], *Xi Wu*[1], *Jie Mao*[2]

[1] Guangxi Key Laboratory of Automobile Components and Vehicle Technology, Guangxi University of Science & technology, Liuzhou 545000, China;
[2] Guangdong Institute of New Materials, Key Lab of Guangdong for Modern Surface Engineering Technology, Guangdong Academy of Science, Guangzhou 510651, China
[*]E-mail: 630681803@qq.com

Received: 13 July 2019 / *Accepted:* 3 September 2019 / *Published:* 7 October 2019

The capacity attenuation of lithium manganate battery is serious in the process of use, which greatly limits the application of $LiMn_2O_4$ material. In this paper, the properties of $LiMn_2O_4$ material and $Li_{1.5}Al_{0.5}Ge_{1.5}(PO_4)_3$ solid electrolyte material combined in a certain proportion could be researched by X-ray diffractometer, electron scanning microscope, charge-discharge cycle test, AC impedance test and cyclic volt-ampere test. The specific discharge capacity of $LiMn_2O_{4(9:1)}$ and $LiMn_2O_{4(7:3)}$ composite cathode materials at 0.1c rate charge-discharge cycle is 108.5595 $mAh \cdot g^{-1}$, 110.013 $mAh \cdot g^{-1}$, which is lower than that of $LiMn_2O_4$. After 50 cycles, the capacity retention rates of $LiMn_2O_4$, $LiMn_2O_{4(9:1)}$ and $LiMn_2O_{4(7:3)}$ were 63.12%, 83. 22% and 94. 35%, respectively. It is concluded that adding a certain amount of $Li_{1.5}Al_{0.5}Ge_{1.5}(PO_4)_3$ can effectively alleviate the problem of $LiMn_2O_4$ capacity attenuation.

Keywords: $LiMn_2O_4$, $Li_{1.5}Al_{0.5}Ge_{1.5}(PO_4)_3$, $LiMn_2O_4/Li_{1.5}Al_{0.5}Ge_{1.5}(PO_4)_3$ composite cathode materials, performance study

1. INTRODUCTION

LIBs have been diffusely used in portable electronic products such as mobile phones, laptops and digital cameras, which provide great convenience for people's daily life. In the future, LIBs will be critical to the pure electric vehicles field. Cathode materials have a lot of impact on the performance of LIBs, meanwhile, it plays a central role to improve the properties of cathode materials in the development of LIBs. China is rich in manganese resources, the development of manganese-based cathode materials will have a broad space for development. $LiMn_2O_4$ (LMO) cathode material with spinel structure has become the first choice material for LIBs owing to its advantages of non-toxicity, low cost, simple preparation process, high capacity, high discharge voltage and long cycle life[1]. Due

to the destruction of crystal structure caused by Jahn-Teller effect during charge-discharge, the $LiPF_6$ electrolyte is decomposed into corroded LMO material and manganese ions are easily dissolved in electrolyte, which leads to serious capacity attenuation of LMO material during charging and discharging, which limits the large-scale application of LMO material[2-4]. At present, we generally use ion doping to stabilize the crystal structure of LMO material[3-7] and cover other materials on the surface of LMO material to reduce the contact with electrolyte[8-11] to improve the cyclic properties of LMO materials. Although doping and coating methods can enhance the cycling behavior of LMO material, which lead to weak the initial capacity in LIBs[12]. In this paper, the composite cathode material was prepared by mixing LMO material with solid electrolyte material and its properties were studied. $Li_{1.5}Al_{0.5}Ge_{1.5}(PO_4)_3$(LAGP) is a kind of solid-state electrolyte material, which has the advantages of high lithium ion conductivity (10^{-4} $S.cm^{-1}$), wide electrochemical window, stable electrochemical performance and low cost[13].

In this paper, LMO and LAGP were prepared by high temperature solid phase method and then LMO and LAGP were mixed in a certain proportion. The physical properties of cathode materials were observed by X-ray diffractometer and electron scanning microscope. The electrochemical properties of cathode materials were discussed by charge-discharge cycle test, AC impedance test and cyclic volt-ampere test.

2. EXPERIMENTAL

2.1 Preparation of $LiMn_2O_4$

Using the stoichiometric compound of CH_3COOLi and $Mn(CH_3COO)_2$ as the materials, the LMO product could be obtained through the solid-state reaction. In particular, an excess of 10 wt% CH_3COOLi was added to to supplement the volatilization of lithium at high temperature. The mixtures were preheated at 450 ℃ for 7 h and then warmed at 850 ℃ for 40 hours in air. The LMO could be found after the high temperature reaction.

2.2 Preparation of $Li_{1.5}Al_{0.5}Ge_{1.5}(PO_4)_3$

The LAGP glass was acquired by melt quenching method with CH_3COOLi, Al_2O_3, GeO_2 and $NH_4H_2PO_4$ as raw materials. The mixture was obtained by weighing the raw material according to stoichiometric ratio and then mixing it with 450 rpm for 12 h. The mixture was treated at 700℃ for 2 h to obtain a precursor powder. Precursor powder were reground and then heated at1450℃ for2h. The melts were quenched on a stainless steel mold immediately after being removed from the furnace chamber to form transparent glass state. The products were transferred to the furnace and annealed at 900 ℃ for 12 h to eliminate thermal stress and ensure the formation of glass ceramics . Finally, the glass ceramics are ground into powder for experiment.

2.3 Preparation of positive electrode sheet

The $LMO_{(9:1)}$, $LMO_{(7:3)}$ composite cathode materials was prepared by mixing LMO, LAGP at the weight ratio of 9:1 and 7:3. A slurry composed of the cathode materials, conductive carbon black and poly(vinylidene fluoride) was coated on an aluminum foil. All the materials were dissolved in NMP (n-methyl-2-pyrrolidone) with a mass ratio of 80:10:10. After drying at 60℃ in the drying box, the positive electrode sheet with diameter 16mm is cut[14].

2.4 Battery assembly

CR2016 buckle battery was composed in AR glove box with lithium sheet as negative electrode and polypropylene microporous membrane as diaphragm. As shown in Fig.1, the assembly order is positive electrode shell, positive electrode sheet, electrolyte, diaphragm, electrolyte, lithium sheet, stainless steel spacer and negative electrode shell.

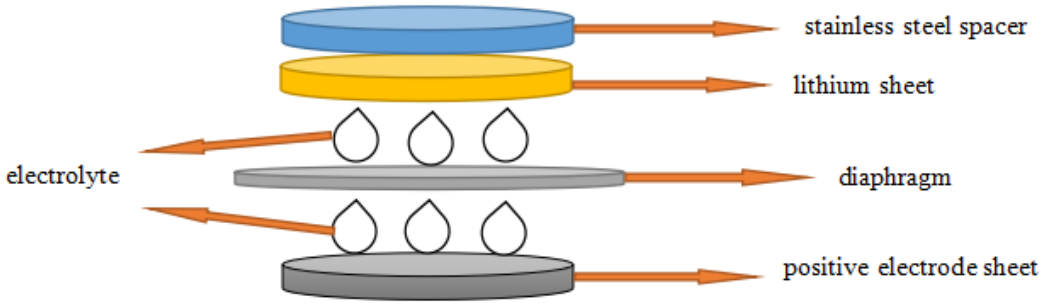

Figure 1. Assembly diagram of battery pack.

2.5 Material characterization

The X-ray diffraction patterns were recorded in the 2θ range of 10°～90° and acquired by an X-ray diffractometer (XRD, Bruker D8 Advance, 40 kV, 30 mA) with Cu Kα radiation. The surface morphology was ascertained by scanning electron microscopy(SEM,∑IGMA). Electrochemical impedance spectroscopy was measured on a CHI660E electrochemical workstation. Its frequency range is 0.01Hz ~10^5Hz and its AC amplitude is 5mV. In order to evaluate the reversibility of the reaction, cyclic voltammetry was used with scanning rate of 0.1mVs^{-1}.

3. RESULTS AND DISCUSSION

3.1. Physical properties of the cathode materials

The XRD patterns about LMO, $LMO_{(9:1)}$, $LMO_{(7:3)}$ which were attained by solid-state reaction were displayed in Fig.2. The spinel structure with the space group of Fd3m (JCPDS 35–0782) can be well confirmed in the XRD spectra of LMO, which not any impurity peaks[14,15]. The

diffraction peak of LAGP is sharp and the strength is high, which indicates that the material has high crystallinity[16-18]. The characteristic peak of the mixture $LMO_{(9:1)}$, $LMO_{(7:3)}$ are still present, indicating that the mixture still belongs to the spinel structure. The addition of LAGP has no effect on the crystal structure of LMO. In particular, $LMO_{(7:3)}$ has obvious abnormal peak, which is the diffraction peak of LAGP.

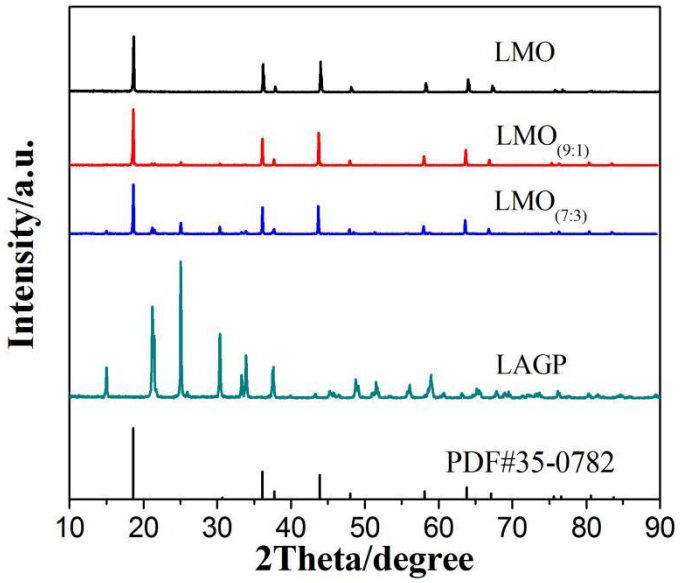

Figure 2. X-ray diffraction patterns of LMO, $LMO_{(9:1)}$, $LMO_{(7:3)}$, LAGP in the 2θ range of 10°~90°.

The SEM diagram of LMO, $LMO_{(9:1)}$, $LMO_{(7:3)}$ are shown in Fig.3. From these images, it can be found that the LMO maintains the favorable spinel structure with uniform granularity. Fig.3(c) obviously shows that the LAGP affects the LMO micro-morphology. Compared with LMO, $LMO_{(7:3)}$ has smaller size and smaller distance between particles. This is convenient for lithium ion shuttle and has a positive effect on electrochemical performance.

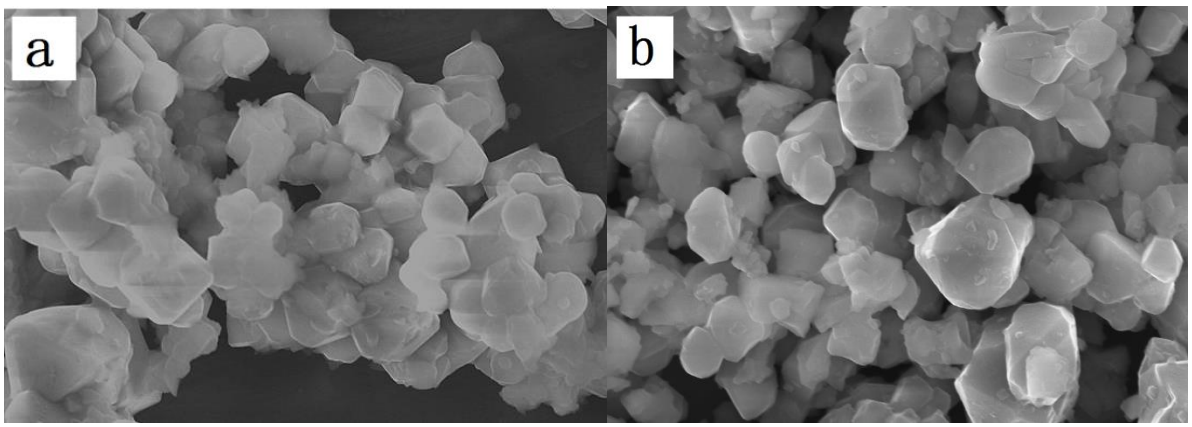

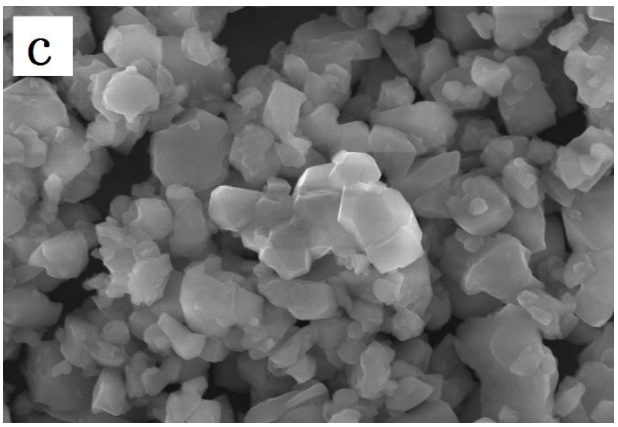

Figure 3. SEM image (Magnification = 20.00 K X) (a) LMO (b) $LMO_{(9:1)}$ (c) $LMO_{(7:3)}$.

3.2. Performance of the battery

The cycling performance curves of LMO, $LMO_{(9:1)}$, $LMO_{(7:3)}$ at 0.1C are presented in Fig.4. Fig.4 evidently demonstrates that the capacity attenuation of LMO is serious. It can be found that LMO $_{(9:1)}$ decays rapidly after 35 cycles. LMO $_{(7:3)}$ possesses not only higher capacity, but also better cycle stability. The reason is that adding LAGP will reduce the contact between LMO and electrolyte to a certain extent, thus reducing the damage to LMO. The initial discharge specific capacity of LMO, $LMO_{(9:1)}$, $LMO_{(7:3)}$ are 118.2471 $mAh{\cdot}g^{-1}$, 108.5595 $mAh{\cdot}g^{-1}$, 110.013 $mAh{\cdot}g^{-1}$, and the discharge specific capacity of the 50th cycle are 74.6326 $mAh{\cdot}g^{-1}$, 90.341 $mAh{\cdot}g^{-1}$, 103.802 $mAh{\cdot}g^{-1}$. It expresses that when a certain amount of LAGP is added, the mass of the active substance decreases and the specific capacity is reduced. After 50 cycles, the capacity retention rates of LMO, $LMO_{(9:1)}$, $LMO_{(7:3)}$ were 63.12%, 83.22%, 94.35%, respectively. From Table 1, we can see that mixing LMO and LAGP with ion doping and coating can achieve the same goal of increasing capacity retention. Although adding a certain amount of LAGP can reduce the capacity of materials, it is of great help to improve the cyclic stability.

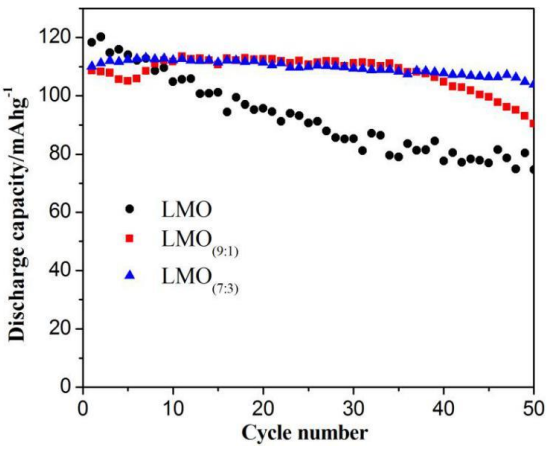

Figure 4. Cycling performance curves of LMO, $LMO_{(9:1)}$, $LMO_{(7:3)}$ at 0.1C and room temperature.

Table 1. Literature overview of improving $LiMn_2O_4$ performance.

Methods	Discharge Conditions	Capacity retention	References
Sc-doped	500cycles at1C	>90%	[1]
Dy-doped	0.1C	96%	[3]
Ce-doped	150cycles at1C	97%	[4]
High temperature calcination in an oxygen atmosphere	500 and 1000 cycles at 1C	94% and 88%	[8]
$FePO_4$ coating	80 cycles	68%	[10]
LaF_3 coating	50 cycles at 2C	99.7%	[11]
LMO and LAGP were mixed	50 cycles at 0.1C	94.35%	This work

The reversible degree of the reaction of the active substance can be judged from the symmetry of the oxidation peak and the reduction peak of the cyclic voltammograms. In the Fig.5, there is one thing in common that two pairs of redox peaks are exhibited in each products between 3.0 V and 4.35 V. It corresponds two-stage intercalation/delamination of Li^+[5]. $LMO_{(9:1)}$, $LMO_{(7:3)}$ displays higher peak current density than LMO at equal scanning rate. The higher crystallinity and lower internal resistance could be found in the former sample. This conclusion is proved in Fig.6. Among them, the peak current density of $LMO_{(7:3)}$ is the highest, and there are two oxidation peaks near 4.08v and 4.26v, and two reduction peaks near 3.85v and 4.06v[14], which indicates that the cycle performance of $LMO_{(7:3)}$ is better.

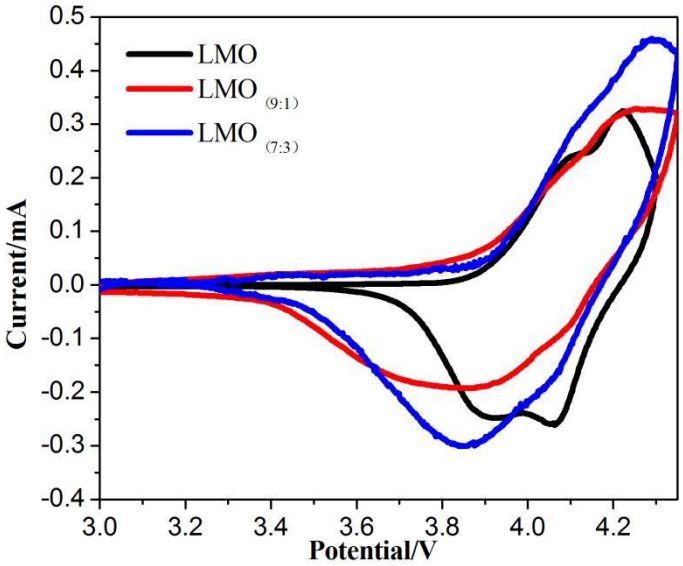

Figure 5. Cyclic voltammograms of LMO, $LMO_{(9:1)}$, $LMO_{(7:3)}$ at a scan rate of 0.1 mV s^{-1} in the 3 ~ 4.35 V range.

Fig.6 is the AC impedance diagram of LMO, $LMO_{(9:1)}$, $LMO_{(7:3)}$. There are two semicircles in the high frequency region and a oblique line in the low frequency region are found in the AC impedance diagram[19]. The intersection point between the semicircle and the real axis is the impedance value[20]. As shown in the equivalent circuit, where Re, Rs, Rct and Zw denote solution resistance, surface film resistance, charge transfer resistance and Warburg resistance, respectively[21]. Table 2 shows the fitted impedance parameters. It can be seen from the table that the impedance value decreases after adding LAGP. It indicates that adding LAGP can increase the lithium ion channel and ameliorate the transport properties of lithium ion at the interface.

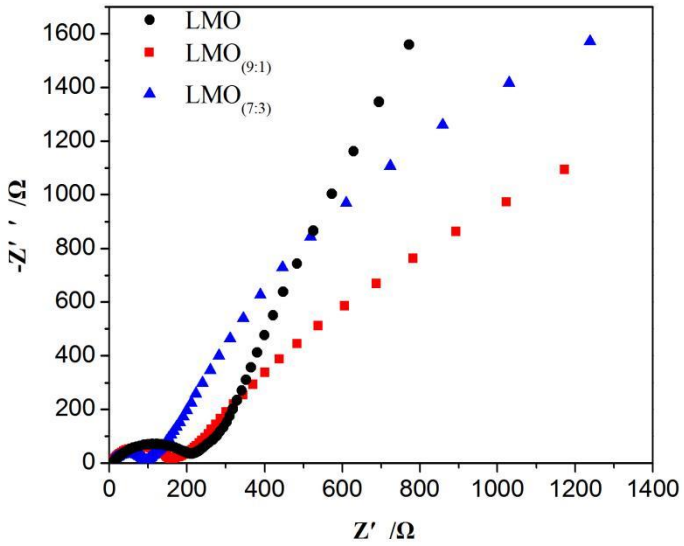

Figure 6. AC impedance diagram of LMO, $LMO_{(9:1)}$, $LMO_{(7:3)}$ in after-cycle state at room temperature.

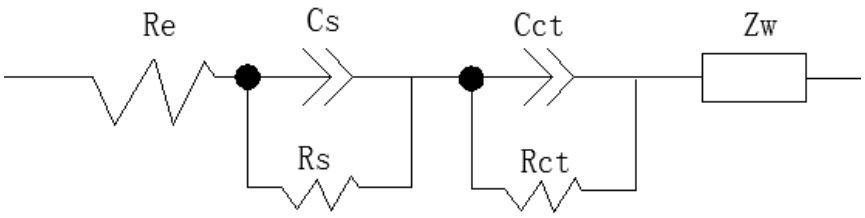

Figure 7. Equivalent circuit model used to fit the data.

Table 2. Impedance parameters evaluated from the EIS data by using the equivalent circuit.

Samples	$R_e(\Omega)$	$R_S(\Omega)$	$R_{ct}(\Omega)$
LMO	4.7	177.1	28502
$LMO_{(9:1)}$	4.9	134.5	319.8
$LMO_{(7:3)}$	5.0	84.3	333.2

4. CONCLUSIONS

In this work, we have repeated engraving a solid-state method to synthesize spinel structure LMO and a melt quenching method to synthesize LAGP. LMO is a spinel structure with a space group of Fd3m and LAGP has good crystallinity. We found that the structure of spinel remained unchanged and the size of material decreased when LAGP was added to LMO. The dense accumulation of particles is instrumental in the shuttle of lithium ions. As shown in Fig.4, it is concluded that the capacity retention rate of $LMO_{(7:3)}$ is 94.35% after 50 cycles, which effectively alleviates the problem of LMO capacity attenuation. The fact that the impedance of $LMO_{(7:3)}$ is lower than that of LMO proves that its reaction is more reversible. In addition, this paper only studies the data of 9:1 and 7:3, and the most suitable amount of LAGP needs to be further explored.

ACKNOWLEDGEMENTS
This work was supported by Fund Project of Guangxi Key Laboratory of Automobile Components and Vehicle Technology, Guangxi University of Science and Technology (No.2017GKLACVTZZ04); Innovation Project of Guangxi University of Science and Technology Graduate Education(YCSW2019210); GDAS' Special Project of Science and Technology Development(N0.2017GDAS CX-0202); Innovation Team Project of Guangxi University of Science and Technology(No.3); Fund Project of the Key Lab of Guangdong for Modern Surface Engineering Technology(No.2018KFKT01).

References

1. S. Bhuvaneswari, U. V. Varadaraju, R. Gopalan, R. Prakash, *Electrochim. Acta*, 301 (2019) 342.
2. H. Y. Zhao, Y. F. Nie, Y. F. Li, T. T. Wu, E. Q. Zhao, J. X. Song, S. Komarneni, *Ceram. Int.*, 45 (2019) 17183.
3. P. Ram, R. Singhal, R. K. Sharma, *Mater. Today*, 4 (2017) 9365.
4. M. Michalska, D. A. Ziółkowska, J. B. Jasiński, P. -H. Lee, P. Ławniczak , B. Andrzejewski, A. Ostrowski, W. Bednarski, S. -H. Wu, J. -Y. Lin, *Electrochim. Acta*, 276 (2018) 37.
5. J. Xiao, H. L. Zhu, Z. Y. Chen, Z. D. Peng, G. R. Hu, *Trans. Nonferrous Met. Soc. China*, 16 (2006) 467.
6. M. Bakierska, M. Świętosławski, K. Chudzik, M. Lis, M. Molenda, *Solid State Ionics*, 317 (2018) 190.
7. M. M. Chen, R. Y. Wu, S. G. Ju, X. X. Zhang, F. Xue, W. H. Xing, *Microporous Mesoporous Mater.*, 261 (2018) 29.
8. Q. Y. Li, J. W. Zhang, C. H. Gong, J. H. Guo, L. G. Yu, J. W. Zhang, *Ceram. Int.*, 45 (2019) 13198.
9. K. Park, J. -H. Park, S. -G. Hong, J. Yoon, S. Park, J. -H. Kim, D. Yoon, H. Kim, Y. -H. Son, J. -H. Park, S. Kwon, *Electrochim. Acta*, 222 (2016) 830.
10. C. B. Qing, Y. Bai, J. M. Yang, W. F. Zhang, *Electrochim. Acta*, 56 (2011) 6612.
11. Q. Zhu, S. Zheng, X. W. Lu, Y. Wan, Q. Q. Chen, J. W. Yang, L. Z. Zhang, Z. G. Lu, *J. Alloys Compd.*, 654 (2016) 384.
12. A. Iqbal, A. M. Khan, T. Wang, D. C. Li, Y. X. Gao, *Int. J. Electrochem. Sci*., 14 (2019) 929.
13. J. Yang, Z. Huang, B. X. Huang, J. Zhou, X. X. Xu, *Solid State Ionics*, 270 (2015) 61.
14. H. M. Wu, J. P. Tu, Y. F. Yuan, Y. Li, X. B. Zhao, G. S. Cao, *Mater. Chem. Phys.*, 93 (2005) 461.
15. K. Hariprasad, N. Naresh, B. N. Rao, M. Venkateswarlu, N. Satyanarayana, *Mater. Today*, 3 (2016) 4040.
16. G. M. Hou, X. X. Ma, Q. D. Sun, Q. Ai, X. Y. Xu, L. N. Chen, D. P. Li, J. H. Chen, H. Zhong, Y. Li,

Z. B. Xu, P. C. Si, J. K. Feng, L. Zhang, F. Ding, L. J. Ci, *ACS Appl. Mater. Interfaces.*, 10 (2018)18610.
17. Z. H. Zhang, S. J. Chen, J. Yang, G. Z. Liu, X. Y. Yao, P. Cui, X. X. Xu, *Electrochim. Acta*, 297 (2019) 281.
18. J. L. Shi, Y. G. Xia, S. J. Han, L. F. Fang, M. Z. Pan, X. X. Xu, Z. P. Liu, *J. Power Sources.*, 273 (2015) 389.
19. Z. M. Zou, Z. J. Li, H. Zhang, X. H. Wang, C. H. Jiang, *J. Mater. Sci. Technol.*, 33 (2017) 781.
20. X. Y. Zhou, M. M. Chen, H. L. Bai, C. W. Su, L. L. Feng, J. M. Guo, *Vacuum*, 99 (2014) 49.
21. X. H. Liang, Y. C. Zhao, D. Han, Q. Q. Chang, M. H. Huang, *Int. J. Electrochem. Sci*., 12 (2017) 9231.